Applications in Engineering Science 10 (2022) 100100

Contents lists available at ScienceDirect

Applications in Engineering Science

journal homepage: www.elsevier.com/locate/apples

Intrinsic modulus and strain coefficients in dilute composites with a Neo-Hookean elastic matrix

Dmytro Ivaneyko [a,b], Jan Domurath [a,d], Gert Heinrich [c], Marina Saphiannikova [a,*]

[a] Leibniz-Institut für Polymerforschung Dresden e. V., Hohe Straße 6, 01069 Dresden, Germany
[b] Institute of Applied Physics, Technische Universität Dresden, 01062 Dresden, Germany
[c] Technische Universität Dresden, Institut für Textilmaschinen und Textile Hochleistungswerkstofftechnik, 01069 Dresden, Germany
[d] Goodyear Innovation Center, 7750 Colmar Berg, Luxembourg

ARTICLE INFO

Keywords:
Elastomer composite
Rigid sphere
Homogenization
Intrinsic modulus
Intrinsic strain coefficients
Strain energy function modification

ABSTRACT

A finite element modelling of dilute elastomer composites based on a Neo-Hookean elastic matrix and rigid spherical particles embedded within the matrix was performed. In particular, the deformation field in vicinity of a sphere was simulated and numerical homogenization has been used to obtain the effective modulus of the composite μ_{eff} for different applied extension and compression ratios. At small deformations the well-known Smallwood result for the composite is reproduced: $\mu_{\text{eff}} = (1 + [\mu]\varphi)\mu_0$ with the intrinsic modulus $[\mu] = 2.500$. Here φ is the volume fraction of particles and μ_0 is the modulus of the matrix solid. However at larger deformations higher values of the intrinsic modulus $[\mu]$ are obtained, which increase quadratically with the applied true strain. The homogenization procedure allowed to extract the intrinsic strain coefficients which are mirrored around the undeformed state for principle extension and compression axes. Utilizing the simulation results, stress and strain modifications of the Neo-Hookean strain energy function for dilute composites are proposed.

1. Introduction

Rubber composites based on an elastomeric matrix reinforced with rigid fillers such as carbon black and silica are widely used in technical applications, for example in tyres, conveyor belts and automotive mats. For a better product performance, it is essential to develop a consistent theoretical description connecting effective material properties of the reinforced rubbers with the underlying chemistry and microstructure (Ivaneiko et al., 2017a). Although about nearly 90 hyperelastic material models are already known at the present time (He et al., 2021), of which only a small number have chemical and microstructural information on rubber materials, the understanding of the characteristics of filled polymer networks with respect to finite element modelling applications is still incomplete. This task becomes extremely complicated in the presence of so-called active particles, which interact with each other and/or with the surrounding polymer chains. Such interactions lead on one hand to appearance of particulate networks (Huber and Vilgis, 1999; Klüppel, 2003; Vilgis et al., 2009) and on the other hand to localization of the flexible chains on the particle surface (Migliorini et al., 2003; Vilgis, 2005; Saphiannikova et al., 2014; Ivaneiko et al., 2016, 2017b). To simplify the problem, we use the simplest hyperelastic model of rubber elasticity (i.e. Neo-Hooke), whose statistical–mechanical derivation is sufficiently known in the framework of a Gaussian network model, and whose applicability is given for moderate strain ratios of the rubber material. Furthermore, we neglect both the particle–particle and particle–matrix interactions, and by doing this consider so-called inactive rigid particles. The influence of the latter on the elastomeric matrix is reduced to the perturbation of applied deformation field, which gives rise to the hydrodynamic amplification of the matrix moduli. Over the years a considerable progress has been achieved in the description of the effective rubber properties at small deformations (Torquato, 2002). However, the influence of the hydrodynamic amplification on the material behaviour in the regime of finite deformations is still far from full understanding.

So, the shear modulus μ of a dilute elastomer composite filled with the rigid spherical particles has been predicted from the shear modulus μ_0 of the polymer matrix by Smallwood (1944)

$$\mu = \mu_0(1 + 2.5\varphi), \tag{1}$$

where φ is the volume fraction of particles. This result was obtained in analogy to the seminal calculations of Einstein (1906, 1911), who predicted the same change in viscosity of a dilute suspension of rigid spheres in a Newtonian matrix fluid. While at small deformations the

* Corresponding author.
E-mail address: grenzer@ipfdd.de (M. Saphiannikova).

https://doi.org/10.1016/j.apples.2022.100100
Received 24 January 2022; Received in revised form 22 March 2022; Accepted 10 April 2022
Available online 20 April 2022

validity of Smallwood's equation is justified, there is a scarce knowledge, how to modify hyperelastic constitutive equations in the regime of finite deformations. It is a common practice in the industry and science of filled rubbers to multiply the strain in non-linear hyperelastic models with the hydrodynamic amplification factor $X = \mu/\mu_0$ (Klüppel, 2003; Kaliske and Heinrich, 1999; Westermann et al., 1999; Meier and Klüppel, 2008; Lorenz et al., 2010; Plagge et al., 2020), which is much higher than the strain amplification factor $a_d = 1/(1-\varphi)$ predicted in the literature (Einstein, 1906; Batchelor and Green, 1972; Smallwood, 1944; Castañeda and Tiberio, 2000; Govindjee and Simo, 1991).

The strain amplification approach used by the elastomer community (Klüppel, 2003; Kaliske and Heinrich, 1999; Westermann et al., 1999; Meier and Klüppel, 2008; Lorenz et al., 2010) is based on the old recommendation of Mullins and Tobin (1965), who wrote in 1965: *A priory it appears more reasonable to consider that the local strains are on average X times greater than the overall strain*. More precisely, the assumption of Mullins and Tobin (1965) requires that instead of the macroscopic extension ratio λ one should use the microscopic extension ratio Λ in the constitutive equation. The microscopic extension ratio is calculated from the external engineering strain $\varepsilon = \lambda - 1$ as

$$\Lambda = 1 + X\varepsilon. \tag{2}$$

Applying relation (2) to the Hooke's law, it has been shown by us (Domurath et al., 2014, 2017) that the concept of Mullins and Tobin violates the energy balance condition, which should be satisfied when performing the homogenization procedure (Torquato, 2002). This means, a great care should be taken, even when the strain amplification factor is used to modify the linear constitutive equations. Performing numerical simulations of polymer melts, filled with rigid spheroidal particles, we understood that the effect of hydrodynamic amplification in these systems can be decomposed into the stress and strain amplification factors (Domurath et al., 2015, 2019, 2020). The emerging concept of stress and strain amplification has been verified in a recent study of stress–strain behaviour of filled rubbers (Plagge and Klüppel, 2017). According to the authors, the stress amplification is of minor importance, especially for large volume fractions of particles.

It is important to point on another drawback of the strain amplification approach proposed by Mullins and Tobin (1965). Eq. (2) is only valid at small deformations and thus, strictly speaking, cannot be applied in the case of finite deformations, where instead of engineering strain ε one should use appropriate finite deformation measures. To clarify this issue, we decided to perform numerical simulations of dilute elastomer composites up to very high deformation ratios along the extension and compression branches. The first question on which we wanted to obtain an answer to was whether the intrinsic modulus increases or decreases at finite deformations and how strongly. The second question was how the applied strain changes along the principle directions and is it possible to relate these changes with those of the intrinsic modulus. The last but not the least, it was desirable to check the consequences of the hydrodynamic amplification on the practically relevant behaviour of the stress–strain curves. Here the evaluation has been done in the terms of true and engineering stresses by comparing the results at constant and strain-dependent intrinsic moduli.

2. Modelling and simulation

We consider a spherical particle of radius a, embedded within a cubic sample of an elastomeric matrix. The filler particle is assumed to be rigid with the shear modulus $\mu_p = \infty$. The elastic matrix is a soft incompressible body with the shear modulus μ_0. For the description of elastic behaviour of matrix let us use the Neo-Hookean law as a constitutive equation.

In the simulations we minimize the stored energy density functional in the computational domain Ω

$$\Pi(\boldsymbol{u}, p) = \int_\Omega \overline{\psi}\, \mathrm{d}\Omega + \int_\Omega p(J-1)\, \mathrm{d}\Omega. \tag{3}$$

Table 1
Volume of particle V_p and its radius a in units of L and the corresponding volume fraction φ.

V_p	a	φ
10^{-2}	0.134	1.25×10^{-3}
10^{-4}	0.029	1.25×10^{-5}
10^{-6}	0.006	1.25×10^{-7}
10^{-8}	0.001	1.25×10^{-9}

The first term in (3) is the isochoric part of the stored strain energy density of the material model. In our case, this is the Neo-Hookean model

$$\overline{\psi} = \frac{\mu_0}{2}(\bar{I} - 3). \tag{4}$$

with the first isochoric invariant of the Cauchy–Green deformation tensors

$$\bar{I} = J^{-2/3} I \tag{5}$$

and $I = \mathrm{tr}(\boldsymbol{C})$ and $J = \det(\boldsymbol{F})$. The deformation gradient is given as

$$\boldsymbol{F} = \frac{\partial \boldsymbol{x}}{\partial \boldsymbol{X}} \tag{6}$$

with $\boldsymbol{x}$ and $\boldsymbol{X}$ being the position vectors in current and reference configurations, respectively. The right Cauchy–Green deformation tensor is defined as

$$\boldsymbol{C} = \boldsymbol{F}^\top \boldsymbol{F}. \tag{7}$$

The second term in (3) enforces the incompressibility constraint, where p is the hydrostatic pressure. To solve the minimization problem (3), we use a standard finite element method (FEM), namely Galerkin method (Großmann and Roos, 2005; Larson and Bengzon, 2013). We use the FEniCS Package for FEM solution of non-linear variational problem.

The task investigated in this study is in analogy to the original problem by Einstein (1906) and Smallwood (1944): uniaxial deformation in the dilute regime. The geometry of the representative volume element (RVE) is a cube with the edge length L and a spherical hole at its centre defined by $\boldsymbol{r} = (0,0,0)$. To reduce the computational effort, the symmetry of the problem is taken into account and Eq. (3) is only resolved on one eighth of the geometry, see Fig. 1a. The considered volume element of the model is V, volume of the particle V_p and volume of the matrix, divided into FEM mesh cells of tetrahedrons, V_{mesh}. The volume fraction of the particles φ is introduced as a ratio of V_p and V

$$\varphi = \frac{V_p}{V} = \frac{V_p}{V_p + V_{mesh}}, \tag{8}$$

being one of the parameter varied in this study (see Table 1).

Fig. 1b shows a sketch of the geometry and the boundary conditions used in this study. On the particle surface a no-slip condition, $\boldsymbol{u} = \boldsymbol{0}$, is applied. The extension and compression of dilute composites is imposed by applying the displacement $\boldsymbol{u}_0$ at the outer surface defined by $x = L/2$. At the symmetry planes, i.e. $x = 0$, $y = 0$ and $z = 0$, symmetry boundary conditions are applied. The two surfaces at $y = L/2$ and $z = L/2$ are traction free.

Introducing macroscopic elongation ratios $\lambda_{i,0}$, that characterize the deformation of macroscopic model in three principal directions x, y and z, the deformation gradient tensor $\boldsymbol{F}_0$ takes a diagonal form

$$\boldsymbol{F}_0 = \begin{pmatrix} \lambda_{x,0} & 0 & 0 \\ 0 & \lambda_{y,0} & 0 \\ 0 & 0 & \lambda_{z,0} \end{pmatrix}. \tag{9}$$

Then the energy stored in elastic composite due to macroscopic deformation is

$$W_{macro} = \frac{\mu_{eff}}{2} \sum_{i=1}^{3} \left(\lambda_{i,0}^2 - 1 \right), \tag{10}$$

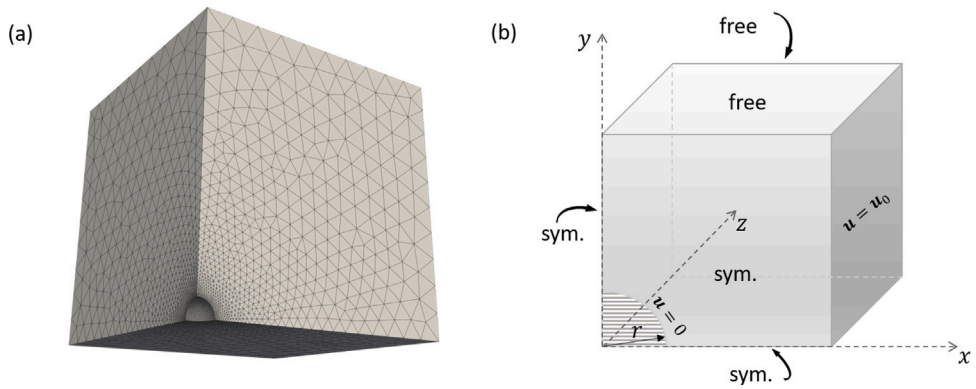

Fig. 1. Elastic matrix with embedded rigid spherical particle at its centre, here the volume fraction $\varphi = 1.25 \times 10^{-3}$ (a) and sketch of the computational domain Ω with boundary conditions (b).

where μ_{eff} is the effective modulus of undeformable hole and soft elastic matrix.

Then the local deformation can be described via a local deformation gradient tensor transformed into the main axis system $\boldsymbol{F}(\boldsymbol{r})$, consisting of its eigenvalues $\lambda_i(\boldsymbol{r})$

$$\boldsymbol{F}(\boldsymbol{r}) = \begin{pmatrix} \lambda_x(\boldsymbol{r}) & 0 & 0 \\ 0 & \lambda_y(\boldsymbol{r}) & 0 \\ 0 & 0 & \lambda_z(\boldsymbol{r}) \end{pmatrix}. \tag{11}$$

The microscopic energy stored in the elastomer composite can be computed as an average of the local energies $w(\boldsymbol{r})$ over the volume V

$$W_{\text{micro}} = \frac{1}{V}\int_V w(\boldsymbol{r})\,\mathrm{d}V = \frac{\mu_0}{2V}\int_{V-V_\text{p}} \sum_{i=1}^{3}\left(\lambda_i^2(\boldsymbol{r}) - 1\right)\,\mathrm{d}V. \tag{12}$$

The r.h.s. of this equation takes into account that the elastic energy is zero inside the volume V_p of rigid (undeformable) particle. The microscopic energy is then set to be exactly equal to its macroscopic equivalent. This homogenization procedure provides the effective modulus in the form

$$\mu_{\text{eff}} = \mu_0 \frac{\frac{1}{V}\int_{V-V_\text{p}} \sum_{i=1}^{3}\left(\lambda_i^2(\boldsymbol{r}) - 1\right)\,\mathrm{d}V}{\sum_{i=1}^{3}\left(\lambda_{i,0}^2 - 1\right)}. \tag{13}$$

The homogenization procedure is carried out for different volume fractions and multiple applied extension and compression ratios, ranging between $\lambda_{x,0} = 0.16 \ldots 4.34$. The extension branch is calculated starting from $\lambda_{x,0} = 1.01$ with a step of 0.01 using at each step the results obtained at the previous extension ratio. The compression branch is calculated in a similar manner starting from $\lambda_{x,0} = 0.99$. We checked that the incompressibility condition $J = 1$ is fulfilled with a very high precision for all applied deformation ratios, as the deviations of J from 1 do not exceed 10^{-4}. The matrix modulus in the Neo-Hookean model is set to be $\mu_0 = 10$ Pa.

3. Intrinsic modulus

It is convenient to analyse the simulation results in terms of the extension dependent intrinsic modulus $[\mu](\lambda)$, defined as the ratio of the specific modulus

$$\mu_{\text{sp}}(\lambda) = \frac{\mu_{\text{eff}}(\lambda)}{\mu_0} - 1 \tag{14}$$

to the volume fraction φ in the limit of vanishingly small values of φ (Larson, 1999)

$$[\mu] = \lim_{\varphi\to 0}\frac{\mu_{\text{sp}}(\lambda)}{\varphi}. \tag{15}$$

Here μ_0 is the matrix modulus and $\mu_{\text{eff}}(\lambda)$ is the modulus of the composite computed according to (13).

Fig. 2a shows the value of μ_{sp}/φ versus the macroscopic extension ratio $\lambda_{x,0}$ for seven different volume fractions: $\varphi = 1.25 \times 10^{-3} \ldots 1.25 \times 10^{-9}$. We noticed if the same results are presented in dependence of the true strain $\epsilon_x = \ln \lambda_{x,0}$ they receive a beautiful symmetrical appearance, as shown on Fig. 2b. The value of μ_{sp}/φ has been calculated at different values of parameter N_{circ} that defines the number of elements along a circle arc on the particle surface. With the increase of N_{circ} the mesh becomes finer. We found that the meshes with $N_{\text{circ}} = 80$ provide a quite accurate estimate of the intrinsic moduli $[\mu] = 2.50 \pm 0.005$ at the dilution exponents $4 \le s \le 7$. An increase of N_{circ} to 100 results in extremely precise values of $[\mu]$, as shown in Table 2. Further increase of N_{circ} at $4 \le s \le 7$ does not affect the results but lets the required computational resources explode. At very high dilutions only the reduced number of elements along a circle arc on the surface of tiny particle could be used: $N_{\text{circ}} = 80$ and 40 at $s = 8$ and 9, respectively.

One can see that there is no difference between the simulation results obtained for four intermediate volume fractions of particles at $N_{\text{circ}} = 100$: $\varphi = 1.25 \times 10^{-4} \ldots 1.25 \times 10^{-7}$. Only the compression zone is gradually enlarged with an increase of the dilution exponent s. In particular, we could reach $\lambda_{x,0} = 0.43$ at $s = 4$ and $\lambda_{x,0} = 0.36$ at $s = 6$. These results for $\lambda_{x,0} < 0.5$ are presented in Fig. 2, but they are hidden behind the curves for $s \ge 7$ being very close to the corresponding results. At very high dilutions with $s \ge 7$, we could model extremely low compression values down to $\lambda_{x,0} \approx 0.16$. The code cannot find a solution for the non-linear boundary problem at lower compression ratios.

Some discrepancy is observed for $\varphi = 1.25 \times 10^{-3}$ at $N_{\text{circ}} = 100$, for $\varphi = 1.25 \times 10^{-8}$ at $N_{\text{circ}} = 80$ and $\varphi = 1.25 \times 10^{-9}$ at $N_{\text{circ}} = 40$. On one side, the composite is not yet dilute for the largest $\varphi = 1.25 \times 10^{-3}$. On the other side, for very diluted cases the reduced number of elements along a circle arc on particle surface affects the accuracy of numerical simulations. The results for intermediate volume fractions are very close, which proves that the simulations are done in the dilute regime, when $[\mu](\lambda)$ is simply equal to $\mu_{\text{sp}}(\lambda)/\varphi$. As the zone of deep compression $\lambda_{x,0} < 0.35$ can be only explored at high dilution, we chose $\varphi = 1.25 \times 10^{-7}$ for a further analysis.

For small values of the extension ratios, i.e. in the linear regime, Smallwood's result for the intrinsic modulus of spherical particles $[\mu] = 2.500$ is reproduced with a high accuracy. This value for the undeformed state at $\lambda_{x,0} = 1.00$ is obtained as an average between the intrinsic moduli calculated at $\lambda_{x,0} = 0.99$ and $\lambda_{x,0} = 1.01$. For details see Table 2.

At higher extension ratios the intrinsic modulus is found to increase quadratically with the true strain, $\epsilon_x = \ln \lambda_{x,0}$. However, the minimum value of $[\mu]$ lies not at $\lambda_{x,0} = 1.00$ but is shifted into the compression region to $\lambda_{\text{min}} = 0.78$. To verify this rather unexpected result, we performed additional simulations. First, as can be seen on Fig. 3a, exactly the same numerical results were obtained when the sample was deformed either along the axis y or the axis z, keeping two other outer

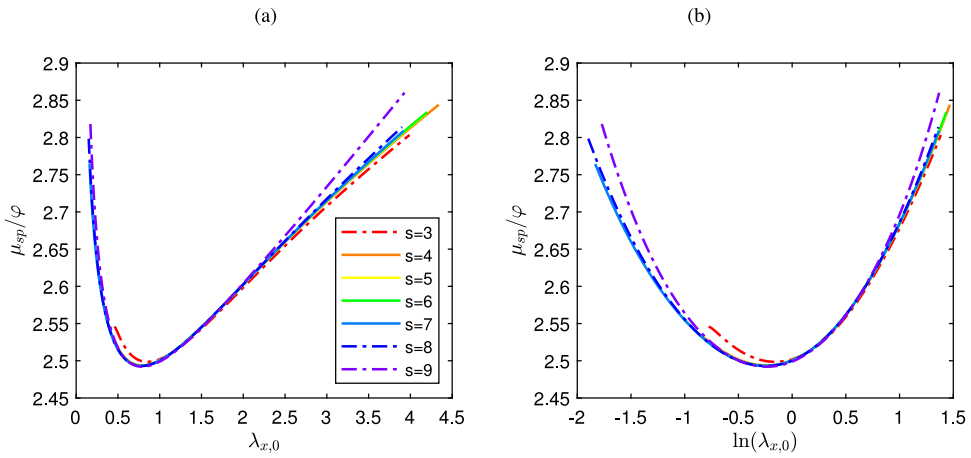

Fig. 2. (a) Dependence of μ_{sp}/φ on the macroscopic extension ratio $\lambda_{x,0}$ along the x-axis for the volume fractions $\varphi = 1.25 \times 10^{-s}$ with the dilution exponent $s = 3 \dots 9$. (b) The same results are plotted in dependence of the true strain $\epsilon_x = \ln \lambda_{x,0}$.

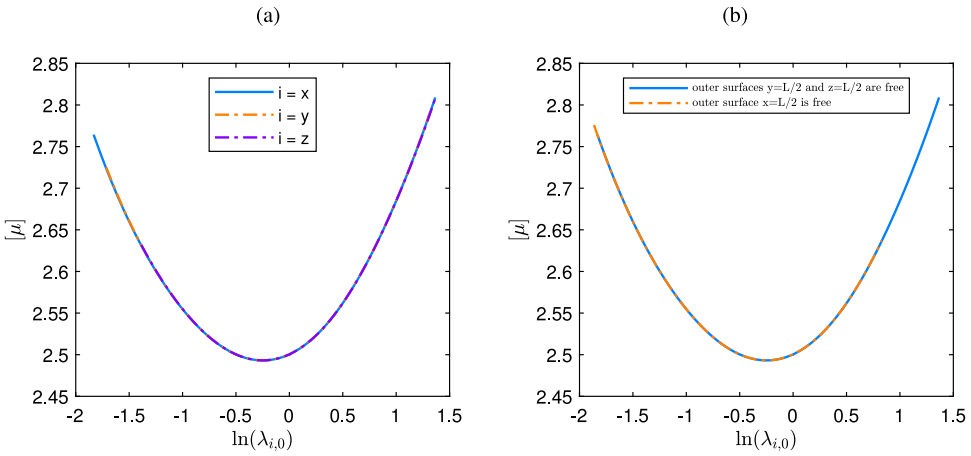

Fig. 3. Dependence of $[\mu]$ on the macroscopic extension ratio $\lambda_{i,0}$ (a) for principal deformation directions along x-, y- and z-axes; (b) for different boundary conditions: the outer surfaces $y = L/2$ and $z = L/2$ are free (blue line) while the deformation is applied along x-axis, the outer surface $x = L/2$ is free (orange dotted line) while equal deformations are applied along y- and z-axes. The volume fraction $\varphi = 1.25 \times 10^{-7}$.

Table 2
Intrinsic modulus $[\mu]$ in vicinity of the undeformed state. Simulations are performed for different values of the volume fraction φ.

φ	$\lambda_{x,0} = 0.99$	$\lambda_{x,0} = 1.01$	$\lambda_{x,0} = 1.00$
1.25×10^{-4}	2.500051	2.501209	2.5006 ± 0.0006
1.25×10^{-5}	2.499891	2.501076	2.5005 ± 0.0006
1.25×10^{-6}	2.499922	2.501108	2.5005 ± 0.0006
1.25×10^{-7}	2.499885	2.501064	2.5005 ± 0.0006
1.25×10^{-8}	2.499619	2.500717	2.5002 ± 0.0005

surfaces free. Second, the equal deformations $\lambda_{y,0} = \lambda_{z,0}$ have been applied simultaneously to two outer surfaces of the sample, keeping the outer surface at $x = L/2$ free. Again, exactly the same numerical results were obtained, see Fig. 3b. This demonstrates a high accuracy of the meshes used in the numerical simulations and an overall correctness of the FEM implemented in the FEniCS Package.

A rather good fit of the simulation data for the intrinsic modulus is provided by the following quadratic dependence as shown on Fig. 4:

$$[\mu] = [\mu]_{\min} + k(\log \lambda_{x,0} - \log \lambda_{\min})^2. \tag{16}$$

Here $[\mu]_{\min} = 2.492$ is the minimum value of $[\mu]$, $\log \lambda_{\min} = -0.2848$ which gives $\lambda_{\min} = 0.752$ and the prefactor $k = 0.1164$. The intrinsic modulus increases up to about 2.81 at $\lambda_{x,0} = 4.00$, that is on about 12%. Though this dependence is rather weak, it can affect the behaviour of the stress–strain curves in practical applications, as we will discuss when considering the regime of high volume fractions. The increase of intrinsic modulus found here is defined by the specific functional form of the Neo-Hookean model. If we would use the strain energy functions with two and more material parameters for description of elastomeric matrix, the homogenization procedure should be performed for multiple deformation modes to enable the extraction of effective material parameters and corresponding intrinsic moduli. Due to the hyperelastic nature of constitutive equations, we expect that all intrinsic moduli shall increase with the deformation. The extent of increase should be at least similar to the Neo-Hookean model or could be even stronger for some intrinsic moduli in the comprehensive material laws (He et al., 2021).

4. Intrinsic strain coefficients

Knowing the intrinsic modulus it is possible to predict the increase of elastic energy upon addition of rigid filler particles in the dilute elastic composites. Another characteristic which attracts a special attention of the research community is the degree of strain amplification. It is believed that knowledge of this characteristic can help to modify the hyperelastic constitutive equations. The strain amplification factor can be introduced in different ways (Domurath et al., 2014, 2017; Plagge and Klüppel, 2017). In numerical simulations it is natural to introduce this factor as an average measure of the elastic field perturbation in

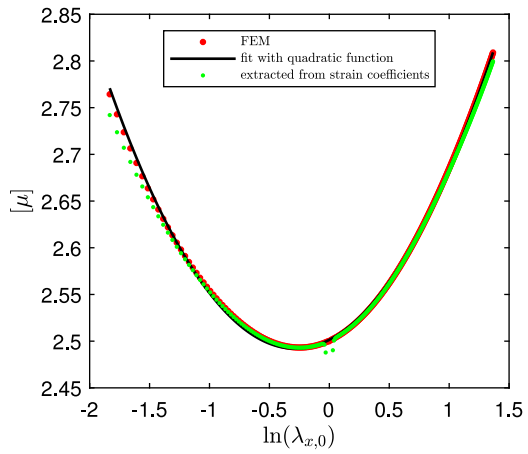

Fig. 4. Fit of the intrinsic modulus $[\mu]$ (red circles) with the quadratic function (16) (black line). Small green circles represent the values of $[\mu]$ extracted with the help of intrinsic strain coefficients according to the relation (20). The volume fraction $\varphi = 1.25 \times 10^{-7}$.

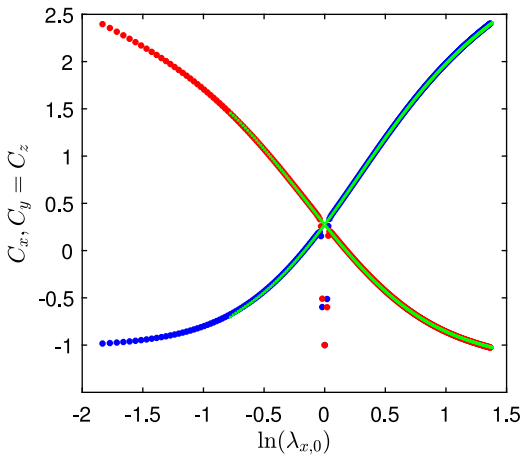

Fig. 5. Intrinsic strain coefficients along the symmetry axis x (blue circles) and in the radial directions y and z (red circles) for the volume fraction $\varphi = 1.25 \times 10^{-7}$. They tend to have the same value 0.25 in the vicinity of $\lambda_{x,0} = 1.0$, which is clearly seen for the volume fraction $\varphi = 1.25 \times 10^{-3}$ (small green circles).

vicinity of the rigid particle. In the case of uniaxial deformation a care should be taken that the amplification factors may differ for principal directions: along the symmetry axis x and the radial directions y and z. In our previous work (Domurath et al., 2015) about the stress and strain amplification in dilute suspensions, we noticed that introduction of the perturbation term $\Delta(\dot\gamma^2) = \dot\gamma^2(\boldsymbol{r}) - \dot\gamma_0^2$, where $\dot\gamma(\boldsymbol{r})$ and $\dot\gamma_0$ are the local and applied deformation rates, helps to receive a meaningful amplification factor. Similarly to dilute suspensions, the intrinsic modulus of dilute elastomer composites can be expressed using appropriate perturbation terms

$$[\mu] = \frac{1}{V_\mathrm{p}} \int_V \frac{\sum_{i=1}^3 (\lambda_i^2(\boldsymbol{r}) - \lambda_{i,0}^2)}{\sum_{i=1}^3 (\lambda_{i,0}^2 - 1)}\, \mathrm{d}V. \tag{17}$$

The derivation of this expression follows directly from the comparison of μ_eff defined by Eq. (13) with its value in the dilute regime $\mu_\mathrm{eff} = \mu_0(1+[\mu]\varphi)$. Besides, it is taken into account that $\lambda_i^2(\boldsymbol{r}) - 1 = 0$ inside V_p, the volume of rigid particle. Note that $[\mu] = 0$ in the limiting case when there is no embedded particles $V_\mathrm{p} = 0$ and the elastic field becomes unperturbed, i.e. $\lambda_i(\boldsymbol{r}) = \lambda_{i,0}$ for any $\boldsymbol{r}$.

In analogy to the expression (17) for intrinsic modulus, the amplification coefficients for the extension ratios along three principal axes $i = x, y, z$ shall be defined as follows

$$C_i = \frac{1}{V_\mathrm{p}} \int_V \frac{\lambda_i^2(\boldsymbol{r}) - \lambda_{i,0}^2}{\lambda_{i,0}^2 - 1}\, \mathrm{d}V, \tag{18}$$

where $\lambda_i^2(\boldsymbol{r})$ are the eigenvalues of the local right Cauchy–Green deformation tensor $\boldsymbol{C}(\boldsymbol{r})$. As the FEniCS Package provides only the principal invariants of the tensors, the characteristic polynomial (eq. (1.169) from Holzapfel (2000)) has been solved for the tensor $\boldsymbol{C}(\boldsymbol{r})$ to extract its eigenvalues $\lambda_i^2(\boldsymbol{r})$. Initially, we found relatively large fluctuations of the amplification coefficients in the radial direction, these can be attributed to uncertainty in the assignment of the local principle axes. Due to the uniaxial symmetry around the axis x, the amplification coefficients C_y and C_z should be equal. Therefore, we averaged simulation results in the radial direction to improve the reliability

$$C_y = C_z = \frac{1}{2V_\mathrm{p}} \int_V \left[\frac{\lambda_y^2(\boldsymbol{r}) - \lambda_{y,0}^2}{\lambda_{y,0}^2 - 1} + \frac{\lambda_z^2(\boldsymbol{r}) - \lambda_{z,0}^2}{\lambda_{z,0}^2 - 1} \right] \mathrm{d}V. \tag{19}$$

Fig. 5 shows the values of C_x and $C_y = C_z$ for two volume fractions $\varphi = 1.25 \times 10^{-7}$ and 1.25×10^{-3}. Similar to the intrinsic modulus, C_i do not depend on the volume fraction φ and therefore can be named intrinsic strain coefficients. C_x is an increasing function of the true strain $\epsilon_x = \ln \lambda_{x,0}$, whereas C_y and C_z decrease with ϵ_x. Two curves cross exactly in the vicinity of $\lambda_{x,0} = 1.0$, where $C_x = C_y = C_z \approx 0.25$. Due to numerical uncertainties at very low volume fractions, there are some runaway values close to $\lambda_{x,0} = 1.0$ but at higher volume fractions like $\varphi = 1.25 \times 10^{-3}$ (small green circles) the cross-point is well-defined. At large elongational strains C_x tends to 2.5, while the radial intrinsic coefficients seem to approach -1.0. The situation is mirrored at large compressive strains: $C_y = C_z$ tend to 2.5, while C_x gradually approaches -1.0. Though a negative value of the intrinsic strain coefficient looks somewhat unusual, it is not unprecedented. For example, negative values of the intrinsic viscosity can be found at high shear rates for strongly shearing fluids (Domurath et al., 2015).

The intrinsic strain coefficients can be related to the intrinsic modulus

$$[\mu] \sum_{i=1}^3 (\lambda_{i,0}^2 - 1) = \sum_{i=1}^3 C_i (\lambda_{i,0}^2 - 1), \tag{20}$$

as follows from comparison of Eqs. (17) and (18). We used the above relation to estimate the values of $[\mu]$ by yet another approach. They are plotted as small green circles on Fig. 4 and appear to be quite close to the values extracted from the effective modulus (13).

Also we tried to find a relation behind the mirror-symmetry of C_i. It follows from the incompressibility condition that

$$(C_x - 1)(\lambda_{x,0} + 1) = 2(C_y - 1)\lambda_{x,0}^2. \tag{21}$$

However, this condition fails totally to describe the simulation results, which is rather expected, because to obtain the intrinsic coefficients not the local extension ratios are averaged but their squares. The best relation which was found after some trials is as follows

$$(C_x + 2)(\lambda_{x,0} + 1) = 2(C_y + 2)\lambda_{x,0}^2. \tag{22}$$

Applying this relation to Eq. (20) allows to separate the strain coefficients

$$C_x = \frac{([\mu] + 2)(\lambda_{x,0} + 1 - 2\lambda_{x,0}^{-1})}{(\lambda_{x,0} + 1)(1 - \lambda_{x,0}^{-3})} - 2. \tag{23}$$

$$C_y = \frac{([\mu] + 2)(\lambda_{x,0} + 1 - 2\lambda_{x,0}^{-1})}{2(\lambda_{x,0}^2 - \lambda_{x,0}^{-1})} - 2. \tag{24}$$

These two expressions predict larger negative values of C_x/C_y in the compression/elongation region, as can be seen from Fig. 6. What is clear, it is not possible to predict the relation between C_i from the incompressibility condition (21) for a macroscopic sample.

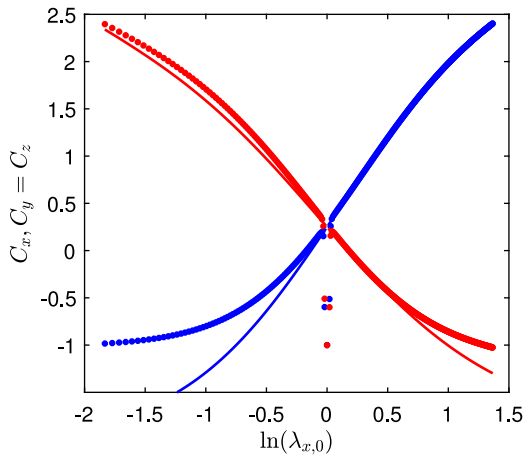

Fig. 6. Intrinsic strain coefficients along the symmetry axis x (blue circles) and in the radial directions y and z (red circles) for the volume fraction $\varphi = 1.25 \times 10^{-7}$. The strain coefficients extracted with the help of relation (22) are presented by the lines of corresponding colours.

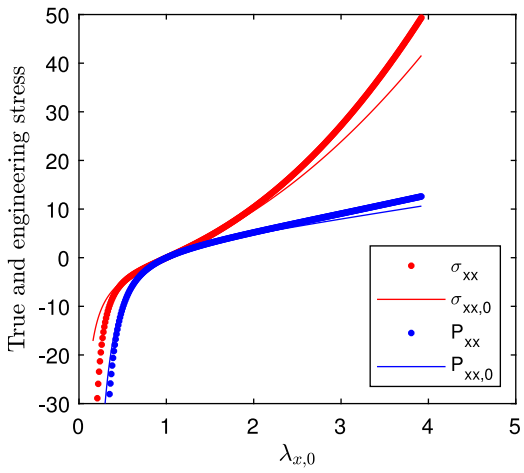

Fig. 7. Dependence of the true stress σ_{xx} (thick red lines) and engineering stress P_{xx} (thick blue lines) on the extension ratio $\lambda_{x,0}$. The corresponding stresses $\sigma_{xx,0}$ and $P_{xx,0}$ for the reference system with constant $[\mu] = 2.50$ are represented by thin red and blue lines. The volume fraction $\varphi = 0.3$.

5. Stress and strain amplification approaches

In the dilute regime $\mu_{\text{eff}} = \mu_0(1 + [\mu]\varphi)$ and the macroscopic strain energy function (10) can be represented as

$$W_{\text{macro}} = \frac{\mu_0}{2}(1 + [\mu]\varphi) \sum_{i=1}^{3} (\lambda_{i,0}^2 - 1). \tag{25}$$

Alternatively, using Eq. (20), it can be shown that

$$W_{\text{macro}} = \frac{\mu_0}{2} \sum_{i=1}^{3} (1 + C_i\varphi)(\lambda_{i,0}^2 - 1). \tag{26}$$

Hence, the macroscopic strain energy function of the dilute elastomer composites can be represented either using a pure stress amplification approach or a pure strain amplification approach. Studying filled polymer melts, we developed the mixed stress and strain amplification approach (SSAA) (Domurath et al., 2012, 2015), which will also be interesting to apply to the elastomer composites. For that let us introduce the stress amplification factor X, defined as the ratio of the composite modulus to the matrix modulus, in the linear regime of small deformations

$$X = \frac{\mu_{\text{eff}}}{\mu_0} = 1 + 2.5\varphi. \tag{27}$$

Inserting this factor in (26), we arrive to

$$W_{\text{macro}} = X\frac{\mu_0}{2} \sum_{i=1}^{3} (1 + (C_i - 2.5)\varphi)(\lambda_{i,0}^2 - 1). \tag{28}$$

In the previous section, we have shown that the largest value of C_i is bounded to 2.5 and thus $C_i - 2.5$ is always negative. This poses a question, whether the mixed stress–strain representation makes sense in the case of hyperelastic matrix.

The findings of Eq. (25) are based on the simulation results for uniaxial tension and compression. They can be extended to a planar tension geometry, also called a pure shear, characterized by the diagonal deformation gradient tensor $F = diag[\lambda, 1/\lambda, 1]$. The macroscopic strain energy for this particular deformation is described by Eq. (25) with $\lambda_{x,0} = \lambda$, $\lambda_{y,0} = 1/\lambda$ and $\lambda_{z,0} = 1$, whereby the intrinsic modulus is again given by Eq. (16). Note, as there is no deformation along the z direction, the intrinsic strain coefficient $C_z = 0$ at all $\lambda_{x,0}$, whereas two other coefficients C_x and C_y should be mirrored around $\lambda_{x,0} = 1$, similar as it is shown on Fig. 5. The macroscopic strain energy given by Eq. (25) should be also valid in case of simple shear or biaxial deformations. However, care needs to be taken in defining, which eigenvalue will play the role of $\lambda_{x,0}$ in Eq. (16) for these complex deformations.

6. High volume fractions

Numerical simulations in the present study have been carried for rather low volume fractions to ensure the dilute regime. This allowed to extract the dependence of the intrinsic modulus on the true strain with a very high accuracy. There are a plenty of reinforcement formulas which allow the extension to higher volume fractions relevant to the practical applications (Torquato, 2002; Vilgis et al., 2009). In the limit of vanishing volume fractions, a good formula should reduce to the Einstein/Smallwood result. As we showed in our previous work (Domurath et al., 2015), a mean-field approach in the style of Krieger and Dougherty will lead to the following extension to the higher volume fractions

$$\frac{\mu_{\text{eff}}}{\mu_0} = \left(1 - \frac{\varphi}{\varphi_{\max}}\right)^{-[\mu]\varphi_{\max}}. \tag{29}$$

Expansion of r.h.s. of this equation into the Taylor series results in

$$\frac{\mu_{\text{eff}}}{\mu_0} = 1 + [\mu]\varphi + \frac{[\mu]}{2}\left([\mu] + \varphi_{\max}^{-1}\right)\varphi^2 + O(\varphi^3). \tag{30}$$

Taking the maximum-packing volume fraction of particles equal to its value for the rigid uniform spheres, $\varphi_{\max} \approx 0.64$ (Larson, 1999), not only the formula of Smallwood (1944) up to $O(\varphi^2)$ but also the exact expression of Chen and Acrivos (1978) up to $O(\varphi^3)$ is reproduced

$$\frac{\mu_{\text{eff}}}{\mu_0} = 1 + 2.5\varphi + 5.0\varphi^2. \tag{31}$$

7. Implications for engineering and true stresses

Using the Krieger and Dougherty equation (29) with the strain-dependent intrinsic modulus (16), we shall study in this section the influence of the latter on the Cauchy $\boldsymbol{\sigma}$ and first Piola–Kirchhoff $\boldsymbol{P}$ stress tensors. For incompressible composites, these tensors can be obtained from the macroscopic strain energy function as follows (Holzapfel, 2000)

$$\boldsymbol{\sigma} = -p\boldsymbol{I} + \frac{\partial W_{\text{macro}}}{\partial \boldsymbol{F}}\boldsymbol{F}^T, \qquad \boldsymbol{P} = -p\boldsymbol{F}^{-T} + \frac{\partial W_{\text{macro}}}{\partial \boldsymbol{F}}. \tag{32}$$

In this study the extension and compression of dilute composite samples is imposed by applying the displacement along the axis x and leaving two other outer surfaces free. This means that only the stress components σ_{xx} and $P_{xx} = \sigma_{xx}/\lambda_{x,0}$ have a non-zero value, and the pressure $p = \mu_{\text{eff}}/\lambda_{x,0}$ can be calculated from the condition $\sigma_{yy} = \sigma_{zz} = 0$. Due to

the strain dependence of the intrinsic modulus (16), the true stress σ_{xx} contains two contributions

$$\sigma_{xx} = \mu_{\text{eff}}(\lambda_{x,0}^2 - \lambda_{x,0}^{-1}) + \frac{\partial \mu_{\text{eff}}}{\partial \lambda_{x,0}} (\lambda_{x,0}^2 - 2/\lambda_{x,0} - 3). \quad (33)$$

The second contribution is considerably smaller than the first one, especially at small volume fractions. Fig. 7 shows strain dependences of the true σ_{xx} (red lines) and engineering stresses P_{xx} (blue lines) for the volume fraction $\varphi = 0.3$. As the reference system we chose the dilute elastomer composite with the constant intrinsic modulus $[\mu] = 2.50$. Note that the second term in r.h.s. of the Eq. (33) is equal to zero for the reference system. Comparison of the results obtained with the strain-dependent and constant intrinsic moduli makes clear, that although the strain dependence appears to be rather weak, it affects considerably the behaviour of the stress–strain curves in the regions of strong elongation, $\lambda_{x,0} > 2$ and compression $\lambda_{x,0} < 0.5$. Especially, the true stress becomes strongly underestimated, when the increase of μ_{eff} with strain is neglected. Hence, it is better to take the strain-dependent hydrodynamic reinforcement into account in the practical applications, where the filled elastomers undergo large deformations.

8. Conclusions

In this contribution a numerical study of dilute elastomer composites was performed with the aim to understand, whether the intrinsic modulus deviates at large deformations from the Smallwood's result $[\mu] = 2.5$. For that we first reproduced the Smallwood's result itself using the homogenization procedure which has been applied to a Neo-Hookean elastic solid with embedded rigid spherical particles. In FE simulations the particle is placed in the centre of a cubic simulation cell, which undergoes either uniaxial extension or compression along one of the principle axes. The difficulty here was that the intrinsic modulus does not have a minimum value at vanishingly small strains, i.e. for the undeformed solid. Contrary, the minimum is shifted into the compression region to $\lambda_{\min} = 0.78$, at which $[\mu] = 2.492$. Averaging the values of intrinsic modulus in the vicinity of undeformed state, we were able to reproduce the Smallwood's result with a very high accuracy: $[\mu] = 2.500$ for the volume fractions $\varphi < 1 \times 10^{-3}$. After proving the correctness of the used homogenization approach, the dependence of intrinsic modulus on the true strain has been extracted up to high extension and compression ratios. Interestingly, this dependence can be fitted by a quadratic function of the true stress. This opens a way for modification of the stored energy density in incompressible Neo-Hookean solid filled with rigid spherical particles.

Besides a pure academic interest, the knowledge of strain-dependent intrinsic modulus can be used in practical applications, when the volume fraction of filler reaches the values of 0.3–0.4. For that it should be feeded into one of the formulas describing the hydrodynamic reinforcement at high volume fractions. In the present study we explored the implications of the strain-dependent intrinsic modulus on hand the Krieger–Dougherty equation. Comparison with the reference system, characterized by a constant intrinsic modulus, clearly showed that the true stress becomes largely underestimated in the regions of high deformation if the strain dependence is neglected.

Finally, we applied the homogenization procedure to extract the degree of strain amplification along principle axes. Here it become possible to introduce the intrinsic strain coefficients, which received their names due to independence on the volume fraction. The coefficients attain the same value of 0.25 in the undeformed state but otherwise they are nearly mirrored around this value. Contrary to the intrinsic modulus, which is always positive, the intrinsic strain coefficients may take negative values down to −1.0. Using these coefficients, we proposed yet one more modification of the strain energy function for elastic composites.

Declaration of competing interest

One or more of the authors of this paper have disclosed potential or pertinent conflicts of interest, which may include receipt of payment, either direct or indirect, institutional support, or association with an entity in the biomedical field which may be perceived to have potential conflict of interest with this work. For full disclosure statements refer to https://doi.org/10.1016/j.apples.2022.100100. Marina Saphiannikova reports financial support was provided by Deutsche Forschungsgemeinschaft.

Acknowledgements

Financial support from Deutsche Forschungsgemeinschaft, Germany under grant GR 3725/8-1 and project 380321452/GRK2430 is greatly appreciated.

References

Ivaneiko, I., Toshchevikov, V., Westermann, S., Saphiannikova, M., 2017a. Multiscale modeling approach to dynamic-mechanical behavior of elastomer nanocomposites. In: Stöckelhuber, K.W., Das, A., Klüppel, M. (Eds.), Designing of Elastomer Nanocomposites: from Theory to Applications. In: Advances in Polymer Science, vol. 275, pp. 157–186. http://dx.doi.org/10.1007/12_2016_3.

He, H., Zhang, Q., Zhang, Y., Chen, J., Zhang, L., Li, F., 2021. A comparative study of 85 hyperelastic constitutive models for both unfilled rubber and highly filled rubber nanocomposite material. Nano Mater. Sci. http://dx.doi.org/10.1016/j.nanoms.2021.07.003.

Huber, G., Vilgis, T.A., 1999. Universal properties of filled rubbers: mechanisms for reinforcement on different length scales. KGK - Kautschuk Gummi Kunststoffe 52 (2), 102–107.

Klüppel, M., 2003. The role of disorder in filler reinforcement of elastomers on various length scales. In: Adv. Polymer Sci., vol. 164, pp. 1–86. http://dx.doi.org/10.1007/b11054.

Vilgis, T.A., Heinrich, G., Klüppel, M., 2009. Reinforcement of Polymer Nano-Composites: Theory, Experiments and Applications. Cambridge University Press.

Migliorini, G., Rostiashvili, V.G., Vilgis, T.A., 2003. Polymer chain in a quenched random medium: slow dynamics and ergodicity breaking. Eur. Phys. J. B 33 (1), 61–73.

Vilgis, T.A., 2005. Time scales in the reinforcement of elastomers. Polymer 46 (12), 4223–4229.

Saphiannikova, M., Toshchevikov, V., Gazuz, I., Petry, F., Westermann, S., Heinrich, G., 2014. Multiscale approach to dynamic-mechanical analysis of unfilled rubbers. Macromolecules 47 (14), 4813–4823. http://dx.doi.org/10.1021/ma501159u.

Ivaneiko, I., Toshchevikov, V., Saphiannikova, M., Stöckelhuber, K.W., Petry, F., Westermann, S., Heinrich, G., 2016. Modeling of dynamic-mechanical behavior of reinforced elastomers using a multiscale approach. Polymer 82, 356–365. http://dx.doi.org/10.1016/j.polymer.2015.11.039.

Ivaneiko, I., Toshchevikov, V., Stöckelhuber, K.W., Saphiannikova, M., Heinrich, G., 2017b. Superposition approach to the dynamic-mechanical behaviour of reinforced rubbers. Polymer 127, 129–140. http://dx.doi.org/10.1016/j.polymer.2017.08.051.

Torquato, S., 2002. Random Heterogeneous Materials: Microstructure and Macroscopic Properties. Springer.

Smallwood, H.M., 1944. Limiting law of the reinforcement of rubber. J. Appl. Phys. 15 (11), 758–766. http://dx.doi.org/10.1063/1.1707385.

Einstein, A., 1906. Eine neue Bestimmung der Moleküldimensionen. Ann. Phys. 324 (2), 289–306. http://dx.doi.org/10.1002/andp.19063240204.

Einstein, A., 1911. Berichtigung zu meiner Arbeit: "Eine neue Bestimmung der Moleküldimensionen". Ann Phys. 339 (3), 591–592. http://dx.doi.org/10.1002/andp.19113390313.

Kaliske, M., Heinrich, G., 1999. An extended tube-model for rubber elasticity: Statistical-mechanical theory and finite element implementation. Rubber Chem. Technol. 72 (4), 602–632. http://dx.doi.org/10.5254/1.3538822.

Westermann, S., Kreitschmann, M., Pyckhout-Hintzen, W., Richter, D., Straube, E., Farago, B., Goerigk, G., 1999. Matrix chain deformation in reinforced networks: a SANS approach. Macromolecules 32 (18), 5793–5802. http://dx.doi.org/10.1021/ma990112e.

Meier, J.G., Klüppel, M., 2008. Carbon black networking in elastomers monitored by dynamic mechanical and dielectric spectroscopy. Macromol. Mater. Eng. 293 (1), 12–38. http://dx.doi.org/10.1002/mame.200700228.

Lorenz, H., Meier, J., Klüppel, M., 2010. Micromechanics of internal friction of filler reinforced elastomers. In: Besdo, D., Heimann, B., Klüppel, M., Kröger, M., Wriggers, P., Nackenhorst, U. (Eds.), Elastomere Friction. In: Lecture Notes in Applied and Computational Mechanics, vol. 51, Springer Berlin Heidelberg, pp. 27–52. http://dx.doi.org/10.1007/978-3-642-10657-6_2.

Plagge, J., Ricker, A., Kröger, N.H., Wriggers, P., Klüppel, M., 2020. Efficient modeling of filled rubber assuming stress-induced microscopic restructurization. Internat. J. Engrg. Sci. 151, http://dx.doi.org/10.1016/j.ijengsci.2020.103291.

Batchelor, G.K., Green, J.T., 1972. The determination of the bulk stress in a suspension of spherical particles to order c 2. J. Fluid Mech. 56 (03), 401–427. http://dx.doi.org/10.1017/S0022112072002435.

Castañeda, P.P., Tiberio, E., 2000. A second-order homogenization method in finite elasticity and applications to black-filled elastomers. J. Mech. Phys. Solids 48 (6–7), 1389–1411. http://dx.doi.org/10.1016/S0022-5096(99)00087-3.

Govindjee, S., Simo, J., 1991. A micro-mechanically based continuum damage model for carbon black-filled rubbers incorporating Mullins' effect. J. Mech. Phys. Solids 39 (1), 87–112. http://dx.doi.org/10.1016/0022-5096(91)90032-J.

Mullins, L., Tobin, N.R., 1965. Stress softening in rubber vulcanizates. Part I. Use of a strain amplification factor to describe the elastic behavior of filler-reinforced vulcanized rubber. J. Appl. Polym. Sci. 9 (9), 2993–3009. http://dx.doi.org/10.1002/app.1965.070090906.

Domurath, J., Saphiannikova, M., Heinrich, G., 2014. Non-linear viscoelasticity of filled polymer melts: Stress and strain amplification approach. Macromol. Symp. 338 (1), 54–61. http://dx.doi.org/10.1002/masy.201100118.

Domurath, J., Saphiannikova, M., Heinrich, G., 2017. The concept of hydrodynamic amplification in filled elastomers. KGK - Kautschuk Gummi Kunststoffe 70 (1–2), 40–43.

Domurath, J., Saphiannikova, M., Férec, J., Ausias, G., Heinrich, G., 2015. Stress and strain amplification in a dilute suspension of spherical particles based on a bird-carreau model. J. Non-Newton. Fluid Mech. 221, 95–102. http://dx.doi.org/10.1016/j.jnnfm.2015.04.002.

Domurath, J., Ausias, G., Férec, J., Heinrich, G., Saphiannikova, M., 2019. A model for the stress tensor in dilute suspensions of rigid spheroids in a generalized Newtonian fluid. J. Non-Newton. Fluid Mech. 264, 73–84. http://dx.doi.org/10.1016/j.jnnfm.2018.12.004.

Domurath, J., Ausias, G., Férec, J., Saphiannikova, M., 2020. Numerical investigation of dilute suspensions of rigid rods in power-law fluids. J. Non-Newton. Fluid Mech. 280, http://dx.doi.org/10.1016/j.jnnfm.2020.104280.

Plagge, J., Klüppel, M., 2017. A physically based model of stress softening and hysteresis of filled rubber including rate- and temperature dependency. Int. J. Plast. 89, 173–196. http://dx.doi.org/10.1016/j.ijplas.2016.11.010.

Großmann, C., Roos, H.G., 2005. Numerische Behandlung Partieller Differentialgleichungen. Vieweg + Teubner Verlag.

Larson, M., Bengzon, F., 2013. The Finite Element Method: Theory, Implementation, and Applications, Vol. 10, 1st edn. Springer Verlag.

Larson, R.G., 1999. The Structure and Rheology of Complex Fluids. Oxford University Press.

Holzapfel, G.A., 2000. Nonlinear Solid Mechanics. Hoboken, NJ, USA, John Wiley & Sons Ltd..

Domurath, J., Saphiannikova, M., Ausias, G., Heinrich, G., 2012. Modelling of stress and strain amplification effects in filled polymer melts. J. Non-Newton. Fluid Mech. 171–172, 8–16. http://dx.doi.org/10.1016/j.jnnfm.2012.01.001.

Chen, H.-S., Acrivos, A., 1978. The effective elastic moduli of composite materials containing spherical inclusions at non-dilute concentrations. Int. J. Solids Struct. 14 (5), 349–364. http://dx.doi.org/10.1016/0020-7683(78)90017-3.